JOURNAL OF MATERIALS SCIENCE 11 (1976) 1041–1065

Structure and properties of polyethyleneterephthalate crystallized by annealing in the highly oriented state

Part 1 *Morphological structure as revealed by small-angle X-ray scattering*

E. W. FISCHER, S. FAKIROV†
Institut für Physikalische Chemie der Universität Mainz, 65 Mainz, Germany, and "Sonderforschungsbereich 41" Mainz/Darmstadt, Germany

The structure of polyethyleneterephthalate bristles drawn about five times in the amorphous state and subsequently crystallized at temperatures between 100 and 260° C has been studied by means of small-angle X-ray scattering. In addition density, heat of fusion and wide-angle scattering behaviour were measured. For comparison, similar experiments were carried out with undrawn samples. The results showed that the degree of crystallinity of PET cannot be calculated from density data on the basis of a simple two-phase model, since the effective densities ρ_c^* and ρ_a^* of the crystalline and amorphous regions depend strongly on crystallization and drawing conditions. With rising crystallization temperature the size of the mosaic blocks building up the crystalline layers and their longitudinal mutual order increase whereas the volume fraction of the crystalline region is only rather slightly effected by the annealing temperature. The difference between the effective density ρ_c^* and the "X-ray density" ρ_c of the crystalline layers is supposed to be caused by lattice vacancies in the boundaries of the mosaic blocks.

1. Introduction

The crystallization process of oriented macromolecules subjected to strain or stress is of considerable interest from two points of view: It occurs very often in film or fibre processing and influences the technological properties of the polymeric material. On the other hand, the questions involved in the crystallization behaviour of oriented chain molecules are also relevant with regard to many basically important problems of polymer physics like chain folding, extended-chain crystallization and the nature of the amorphous state.

Obviously, there are three sets of problems related to the crystallization of oriented macromolecules: (i) the mechanism of transition from the oriented amorphous to the oriented crystalline state; (ii) the morphological structure and the nature of the disordered regions after crystallization; and (iii) the relationship between these structures and the properties of the oriented partially crystallized samples.

The thermodynamics and kinetics of oriented crystallization has been treated by several authors [1–8], who tried to correlate the observed changes of melting point and crystallization rate to the orientation function of the chain sequences and to the applied stress. There are still fundamental arguments, however, about the nature of the nucleation process and the subsequent crystal growth. Some of the treatments are based on the traditional fringed micelle model, where the promotion of crystallization by the orientation and parallelization of the chains is quite obvious. In contrast to this idea, Keller and Machin [7] proposed that the nucleation process is associated with the formation of extended-chain crystals

† Present address: University of Sofia, Faculty of Chemistry, Sofia-26, Bulgaria.

from the oriented molecules and that lamellar crystals grow by chain folding onto those nuclei. Again another conclusion is drawn by Yeh and Geil [8] from the electron microscopical studies of strain-induced crystallization of polyethyleneterephthalate. They assume that the crystallization process results primarily from the rotation, alignment and the perfection of internal order of prefolded, paracrystalline nodules originally present in the amorphous material.

A similar controversy situation exists with regard to the structure of the oriented crystallized polymers. Here especially the nature of the "amorphous" regions is uncertain. We will consider the various proposed models during the discussion of our results.

Mechanical properties of drawn PET have been studied by many authors [9–13]. In many cases, however, no additional structure studies with the same samples have been carried out. The relationship between structure and properties has been discussed by Bonart [9], Peterlin [10], Ward [11], Samuels [12] and others [13].

The main purpose of our studies was the investigation of the dependence of the structure on the annealing conditions, the effect of structure on melting behaviour and on the mechanical properties. In the first part we report the results of the structure studies as revealed by small-angle X-ray scattering, wide-angle scattering and density measurements. The thermal and mechanical properties are described in subsequent papers.

2. Experimental

2.1. Samples

The starting material was 1 mm thick, commercial undrawn, amorphous (by X-ray and density measurements) bristles of PET with molecular weight $\bar{M}_\eta = 26\,000$. They were drawn by an Instron machine with a rate of 0.02 cm min^{-1}. The drawing temperature was 65° C and, therefore, slightly below T_g which is reported to be 67° C for the amorphous bulk polymer [14]. The drawing proceeded as long as all material passes through the neck, which corresponds to a draw ratio of about 5.5:1 and a final diameter of about 0.5 mm. The drawn fibres were isothermally annealed with fixed ends and with an additional restrain of 7 to 10% to ensure that the fibres were not loose during the annealing. The annealing took place for 6 h in a continually pumped glass tube submerged in a oil bath with temperature constant within ± 0.3° C. The annealing temperatures (T_a) were: 100, 120, 140, 160, 180, 200, 220, 240, 250, 255 and 260° C.

Another series of samples was prepared by annealing at 240 or 255° C for different annealing times (t_a) 1, 10, 100, 1000 and 10 000 min. The anneals of 1 and 10 min duration were performed without pumping, e.g. in an air atmosphere.

For comparison, undrawn PET bristles of the starting material were also annealed (with free ends) in the same glass tube and for the same time. All the samples were air-quenched after annealing. Some samples were also prepared by slowly cooling (6° C h^{-1}) after annealing at 255 and 260° C.

2.2. Methods

The small-angle X-ray scattering (SAXS) measurements were carried out with Ni-filtered Cu$K\alpha$-radiation using a scintillation counter. The small-angle intensity was measured using a slit collimated diffractometer from Rigaku-Denki, Japan. Scattering curves were taken with the fibre axes parallel as well as perpendicular to the slit. The absolute value of the scattered intensity was obtained by calibration with a standard sample† [15]. The counting rate was chosen in such a way that the mean square error of each measured value was no more than 2%. In addition, photographic SAXS patterns were obtained by means of a pin-hole type camera (Kiessig camera). The photometer traces were obtained on a Joyce–Loebl photometer.

Apparent crystallinities were determined from density and DSC data. The densities of undrawn and drawn samples were measured by means of a gradient column using a mixture of carbon tetrachloride and hexane. The heat of fusion H_f was determined by the Du Pont DSC apparatus, Modell 990. The crystallinity index w_c was calculated from

$$w_c = (\bar{\rho} - \rho_a)/\Delta\rho \qquad (1)$$

where $\Delta\rho = \rho_c - \rho_a$, ρ_a and ρ_c are the densities of the noncrystalline and crystalline regions, $\bar{\rho}$ is the experimental measured value of density. We used the conventional value for $\rho_a = 1.333$ g cm^{-3} and for ρ_c the recently found value of 1.515 g cm^{-3} [17]. For the heat of fusion of fully crystalline

† The authors are indebted to Professor O.Kratky for offering the standard sample used for measurements of absolute scattering intensity.

PET we used the value 5.8 kcal mol^{-1} = 24.3 kJ mol^{-1} [18]. Experimental details will be described in Part 2.

3. Results

3.1. Microstructure as revealed by SAXS

Some of the small-angle X-ray photographs obtained from the drawn, annealed PET fibres are shown in Fig. 1. It can be noticed that the scattering behaviour depends strongly on the annealing conditions. There are not only alterations of the scattering intensity observed, but also changes of the shape of the meridian reflections. This can be demonstrated by the photometer traces in Fig. 2 which show the density distribution along the meridional layer lines of the SAXS patterns obtained from various samples. The width of the small-angle reflection along the layer line decreases with increasing annealing temperature. At 260° C the first indication of a four-point diagram can be observed from the flat intensity minimum at the meridian.

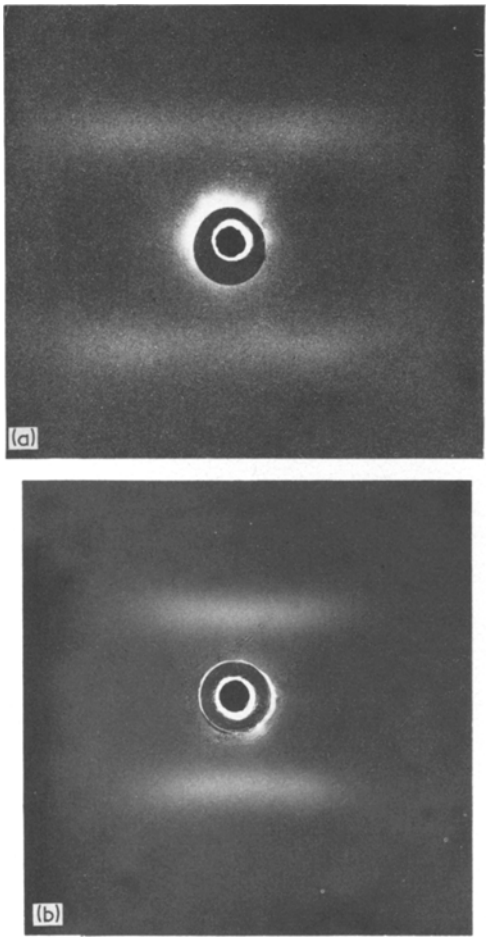

Figure 1 Small-angle X-ray photographs of drawn PET fibres annealed at various temperatures. (a) T_a = 180° C, (b) T_a = 240° C. Fibre axis direction vertical.

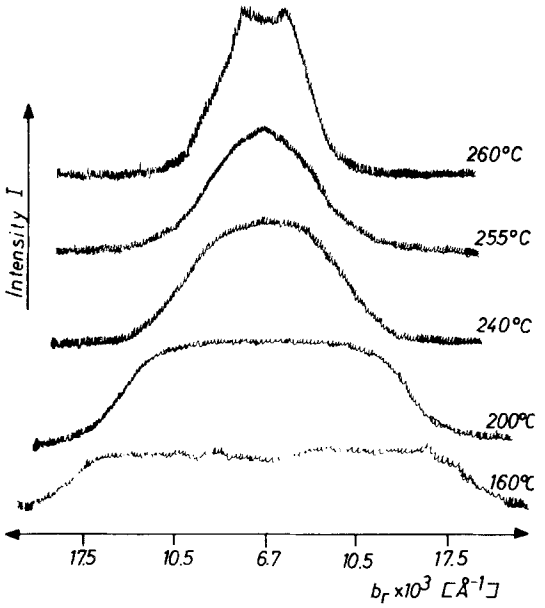

Figure 2 Photometric traces of SAXS meridional reflections measured along the layer lines. The parameter is the annealing temperature.

The alterations of the scattering intensities can be demonstrated most impressively from the scattering curves of Fig. 3. During these measurements the fibre axis was oriented perpendicular to the slit direction of the X-ray camera. A strong increase of the overall intensity is observed with rising annealing temperature. In addition, the angle position of the maxima is shifted to smaller values indicating an increase in the long spacing, L. The variation of L calculated by means of the Bragg equation is plotted in Fig. 4. It shows the generally observed behaviour with regard to the effect of crystallization temperature [16]. At the lowest annealing temperature (T_a = 100° C) no scattering maximum could be observed†. By slowly cooling the annealed samples a somewhat smaller value of L is obtained (see Fig. 14).

The effect of annealing time t_a has also been studied. As shown in Fig. 5, no systematic change in the long spacing, L, can be observed using annealing temperatures of 240 and 255° C. This observation is in remarkable contrast to the data of Zachmann and Schmidt [19] who observed a

† Because of the intensity scale in Fig. 3 the maximum in the scattering curve of the 120° C sample does not emerge, but the long spacing can be determined from the original intensity data.

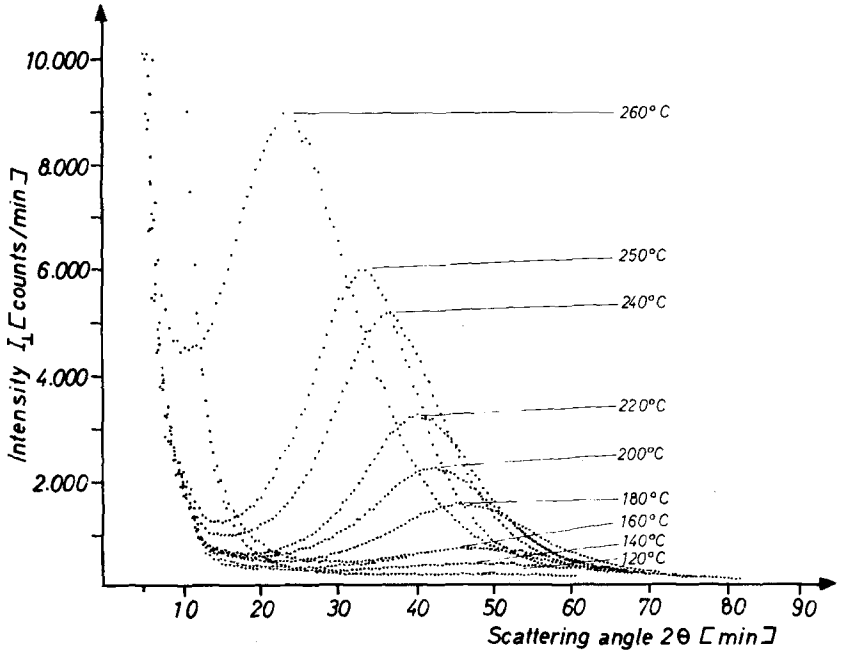

Figure 3 SAXS curves $I_\perp(\theta)$ of drawn PET annealed at various temperatures and measured at room temperatures. Fibre axis is perpendicular to the camera slit. The annealing temperature is indicated.

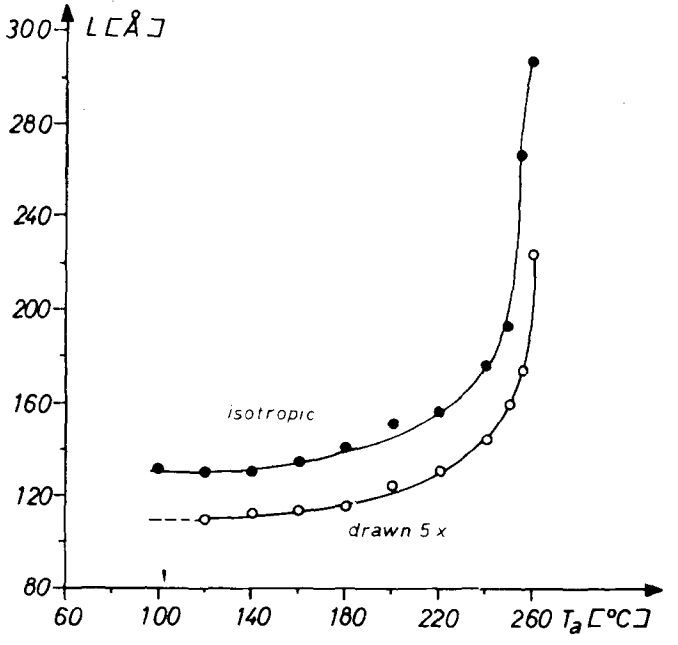

Figure 4 The dependence of long spacing L on annealing temperature T_a for undrawn (•) and drawn (○) fibres.

decrease in L with increasing crystallization time in the case of unoriented PET films. A small increase in intensity (about 20% of the peak intensity) was observed after further annealing for 10 min. No essential changes took place for annealing times between 10 and 10^4 min.

In order to describe quantitatively the intensity changes caused by annealing, the scattering power of the samples has to be measured. It is defined by the mean square density fluctuation $\langle\eta^2\rangle$, when the spatial dependence of the density is given by

$$\rho(\mathbf{x}) = \bar{\rho} + \eta(\mathbf{x}). \qquad (2)$$

The mean square density fluctuation or scattering power can be measured by integrating the scattered

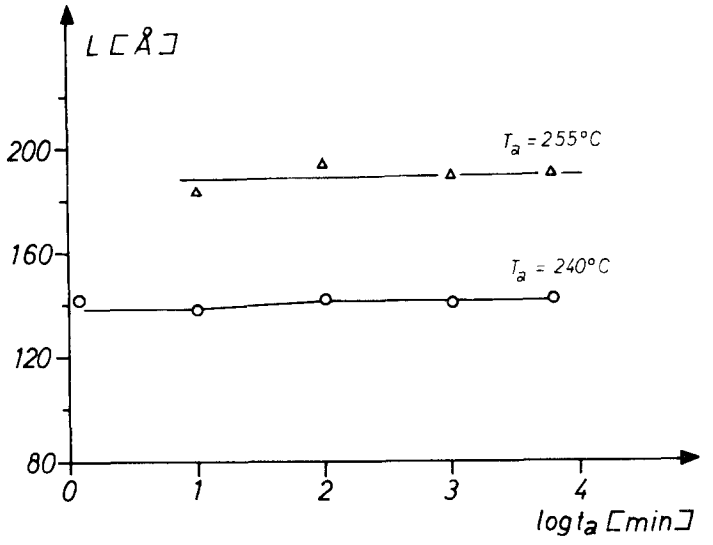

Figure 5 The dependence of long spacing L on annealing time t_a for two annealing temperatures, T_a. (The 1 min sample was annealed in an oil bath.)

intensity $I(\mathbf{b})$ over the whole reciprocal space

$$\langle\eta^2\rangle = \frac{K}{I_0}\int I(\mathbf{b})\,\mathrm{d}^3\mathbf{b}. \tag{3}$$

In the case of an uniaxial oriented sample, $\langle\eta^2\rangle$ can be determined [20, 21] by integrating

$$\langle\eta^2\rangle = \frac{K}{I_0}\,2\pi\int_0^{\infty}\mathrm{I}_{\parallel}(b_r)b_r\mathrm{d}b_r \tag{4}$$

where

$$\mathrm{I}_{\parallel}(b_r)\sim\int_{-\infty}^{+\infty}J(b_r, b_z)\,\mathrm{d}b_z \tag{5}$$

is the intensity measured with the orientation of the fibre axes parallel to the camera slit (b_r, b_z are cylinder co-ordinates of the scattering vector **b**). The constant K has to be determined by comparison with the calibrated sample.

The corresponding scattering curves $I_{\parallel}(b_r)$ are plotted in Fig. 6. Again a strong increase in intensity is observed with rising annealing temperature as could be expected from Fig. 3.

Some difficulties arise in calculating the scattering power according to Equation 4. The integration has to be carried out over the whole angular range and some procedure of extrapolation is necessary for both very small and very large angles. The measured data showed that at angles higher than $2\theta = 100$ to 120 min the scattering intensity remains constant. Therefore, a constant background scattering could be substracted and the integral converged at high angles. The situation at very small angles is more complicated. In contrast to other polymers, e.g. polyethylene single crystals [22] or cellulose and their derivatives [23] for which at the smallest angles the contribution to the scattering power is less than 10% and could be neglected, in the case of PET this is not possible. However, the small-angle X-ray scattering measurements performed by Wendorff and Fischer [24] on melts of polyethylene, PET and other polymers showed that the scattering at very small angles is caused by foreign heterogeneities. This conclusion is supported by the photometric traces of the SAXS patterns of drawn annealed PET fibres (Fig. 2). These traces showing the density distribution along the meridional layer lines do not exhibit a strong increase of the scattered intensity near the meridian. Therefore, one can assume that the increase of $I_{\parallel}(\theta)$ at very small angles originates from the central diffuse scattering due to heterogeneities. The situation is illustrated in Fig. 7, where the separate scattering curves as well as the sum of both are schematically drawn.

The appropriate method for evaluation the scattering power of the PET samples therefore consists of substracting the background scattering due to the heterogeneities from the measured values $I(\theta)$. The resulting scattering curves are shown in Fig. 8. The shape of these curves at small angles now agrees with the photometer traces of the layer lines (Fig. 2).

The same procedure was applied to the scattering curves of undrawn PET. These samples have been also investigated in order to compare the scattering power and long spacings of drawn and

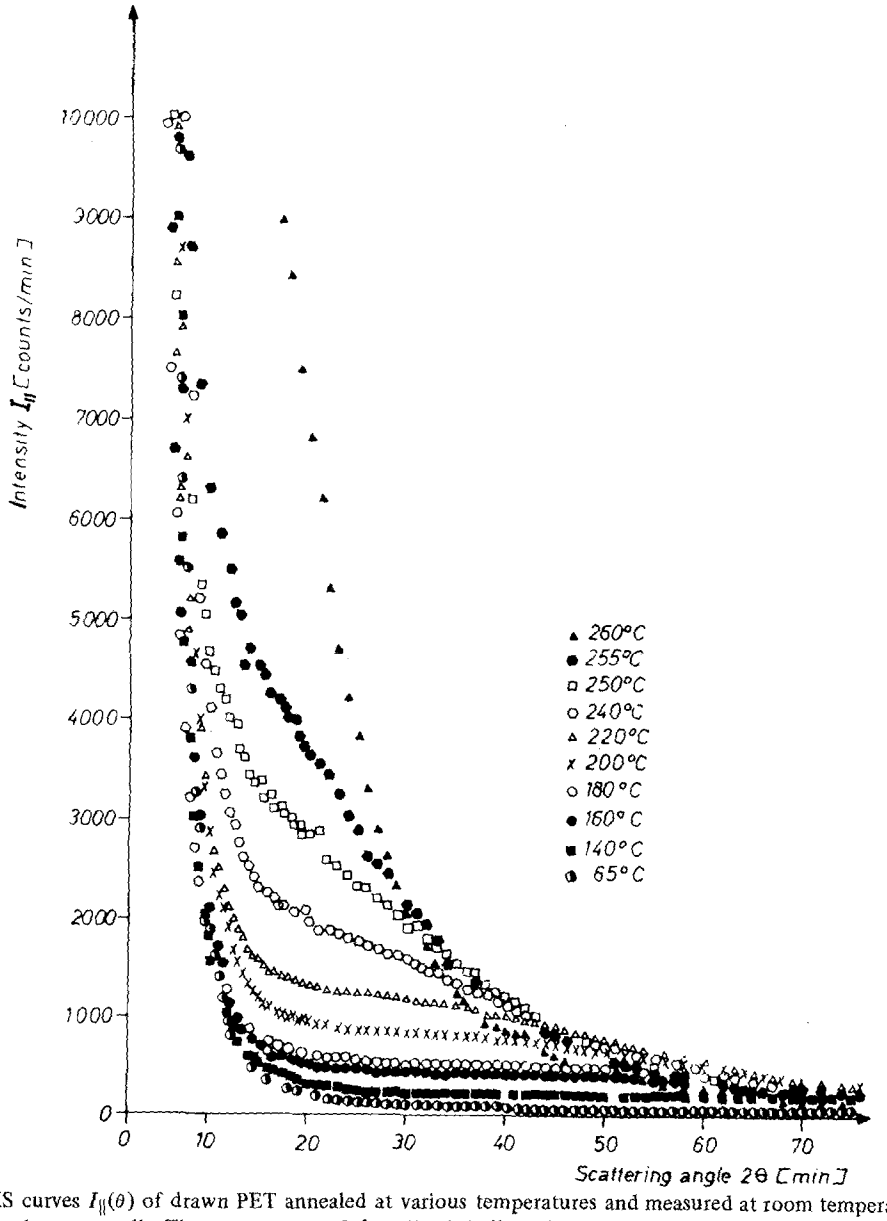

Figure 6 SAXS curves $I_{\parallel}(\theta)$ of drawn PET annealed at various temperatures and measured at room temperature. Fibre axis parallel to the camera slit. The temperature of annealing is indicated.

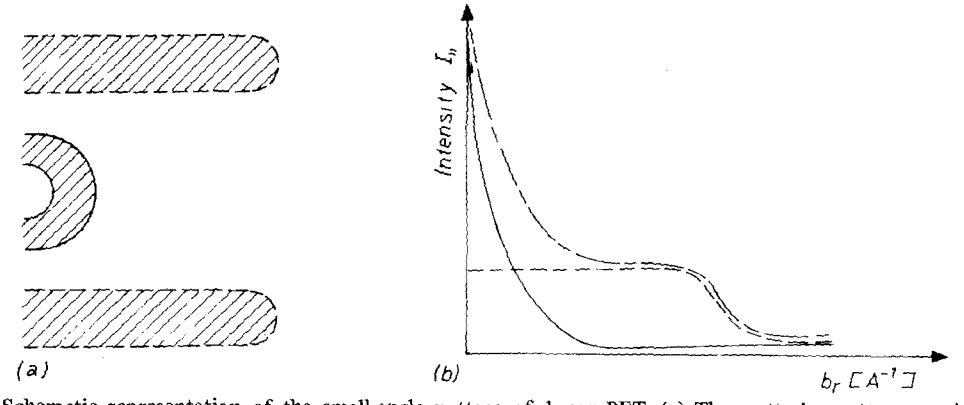

Figure 7 Schematic representation of the small-angle pattern of drawn PET. (a) The scattering pattern consists of a central diffusion scattering and discrete meridional layer lines. (b) The observed (– – –) scattering curve $I_{\parallel}$ (fibre axis parallel to camera slit) is the sum of the diffuse scattering (—) and the meridional scattering (– – –).

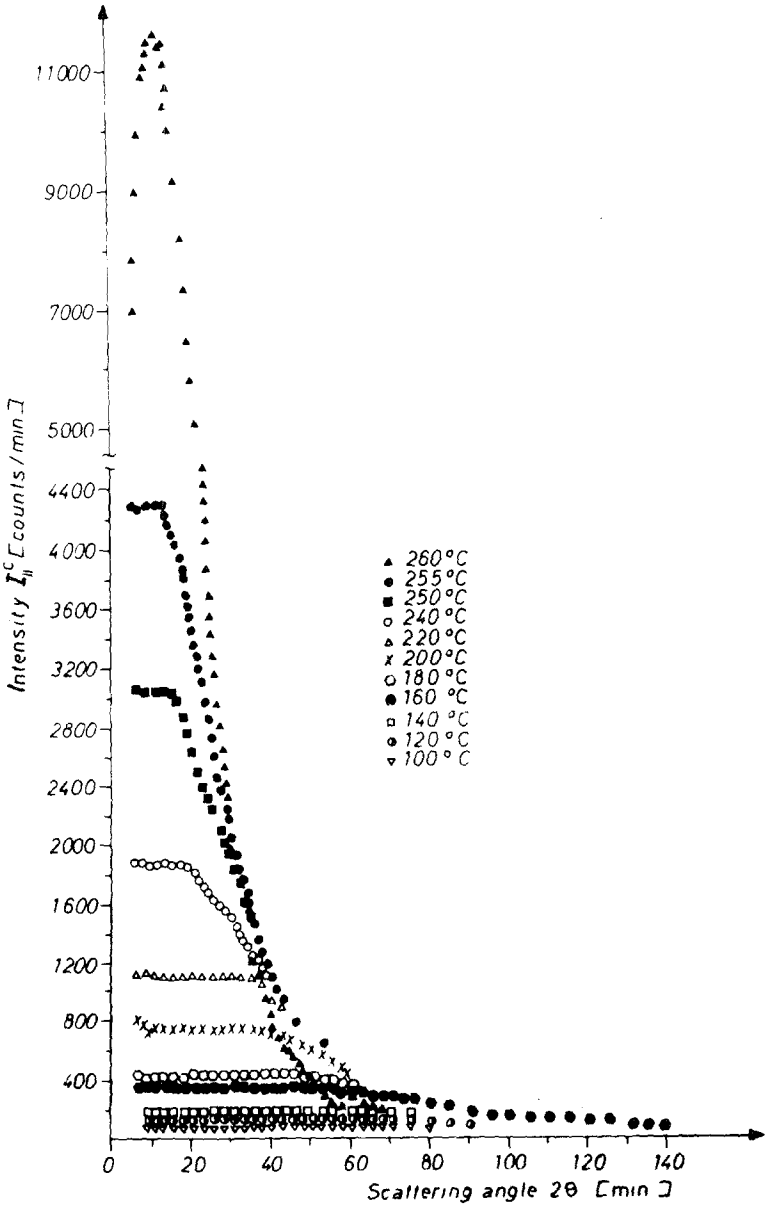

Figure 8 SAXS curves $I_{\parallel}^{c}(\theta)$ corrected with regard to the effect of the central continuous scattering due to foreign heterogeneities of the samples of drawn annealed PET.

undrawn samples annealed under the same conditions and to reconsider the data of other authors [25, 26] obtained for the undrawn polymer. The measured scattering curves are plotted in Fig. 9. Similar effects on intensity are observed to those in the case of drawn samples, see Fig. 3. In Fig. 10 scattering curves are shown after applying the same procedure as for drawn fibres (Fig. 8). Very broad maxima are observed. Intensity curves of the same type were obtained by densitometry of photographic SAXS patterns exhibiting a weak, rather diffuse ring. Nevertheless the scattering curves allowed us to estimate the values of long spacing L for undrawn samples too.

The effect of annealing temperature T_a on the long spacing L for undrawn PET bristles is seen in Fig. 4. The well known relationship between the long period and crystallization temperature is observed. For both drawn and undrawn samples, the increase in L up to $T_a = 240°$ C is not as inten-

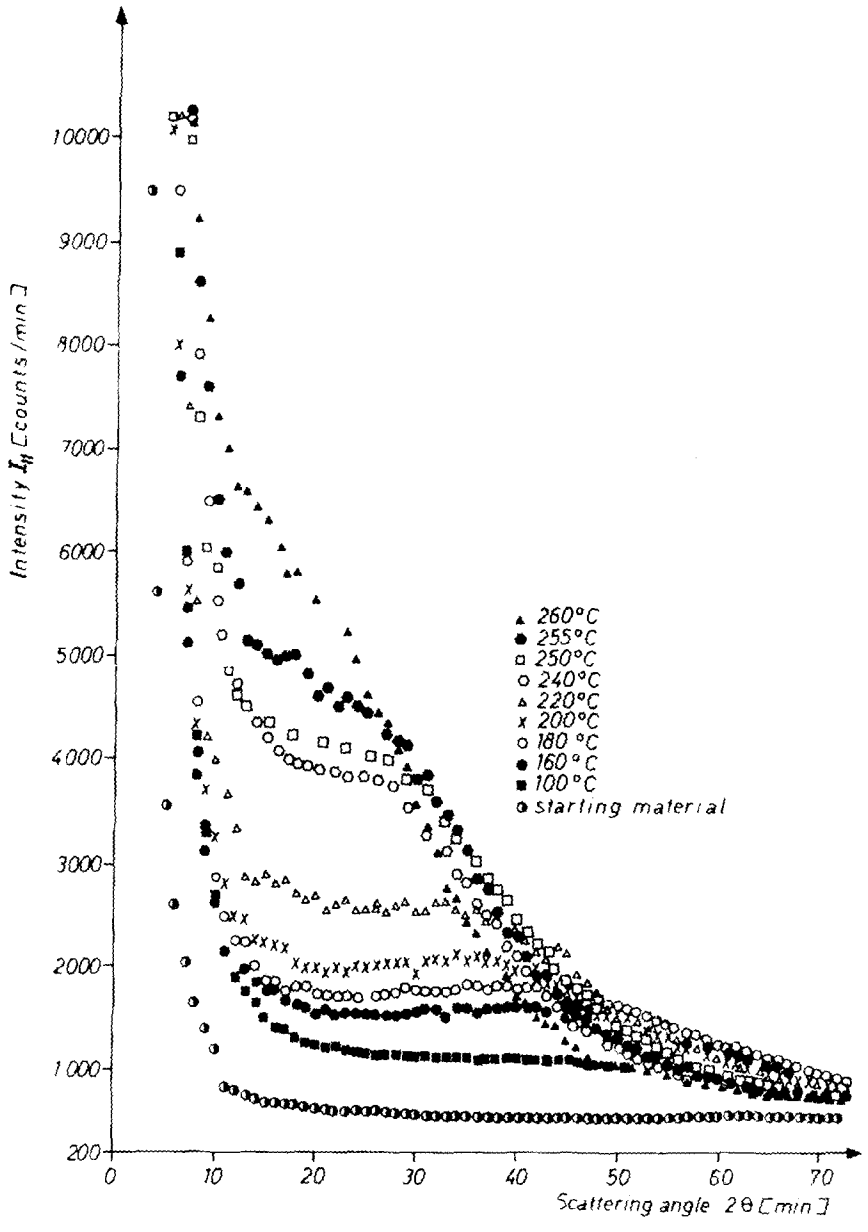

Figure 9 SAXS curves $I_{\parallel}(\theta)$ of undrawn PET annealed at various temperatures and measured at room temperature. The parameter is the annealing temperature T_a.

sive as at T_a higher than 240° C. An interesting characteristic of the undrawn samples can be observed – the values of long spacing in the whole temperature interval of T_a are higher than those for the drawn fibres (Fig. 4).

The values of the mean square density fluctuation evaluated from the scattering curves are plotted in Fig. 11 and tabulated in Table I. As expected from the appearance of the scattering curves the scattering power increases strongly with rising temperature. The values of the undrawn samples for annealing temperatures below about 180° C are higher than those for drawn material.

The data of undrawn samples are in good agreement with those observed by Konrad and Zachmann [25] and by Müller [26] for undrawn, annealed PET films. The values found by these authors are independent of T_a about 1×10^{-3} $(g\,cm^{-3})^2$ higher. We suppose that this difference

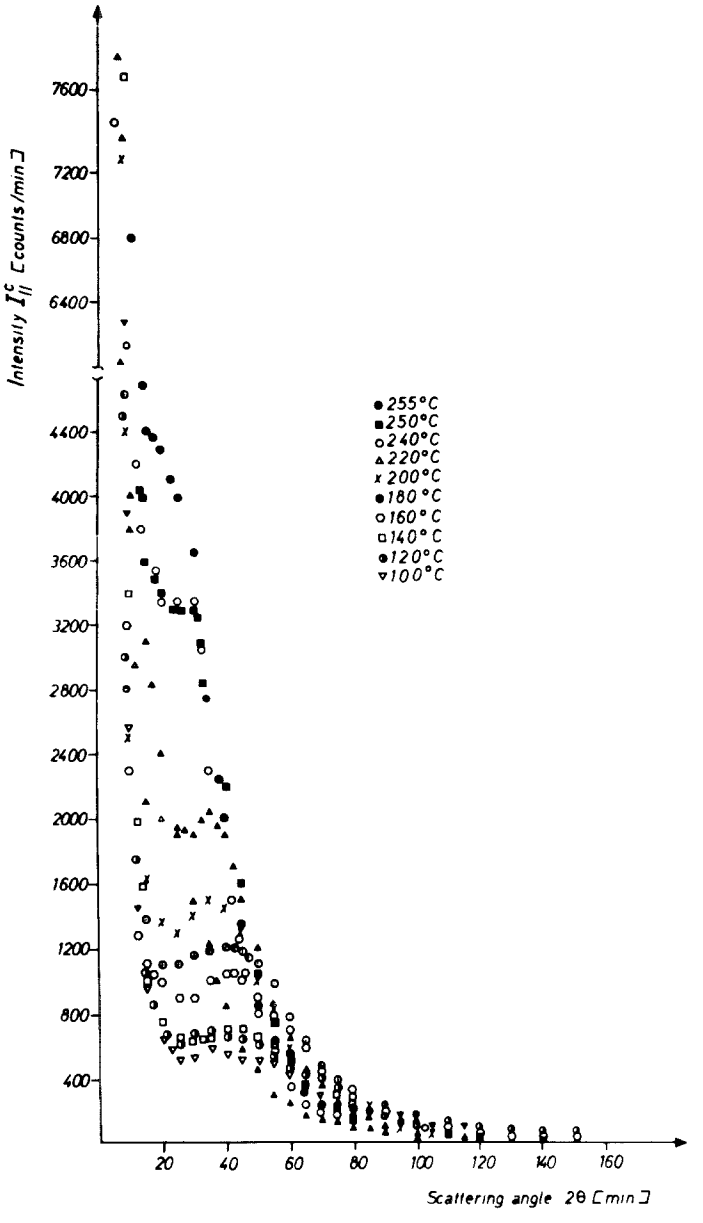

Figure 10 SAXS curves $I_{\|}^{c}(\theta)$ of undrawn annealed PET corrected with regard to the effect of the central continuous scattering due to foreign heterogeneities of the samples.

is due to the scattering effect of the foreign heterogeneities which was not subtracted in their work.

As is well known, the scattering behaviour of polymeric samples in the small-angle range depends not only on the annealing and crystallization conditions but also on the temperature of the sample during measurement. We investigated the effects of measuring temperature for two samples annealed at $T_a = 200$ and 255° C, respectively. The results are shown in Figs. 12 and 13. A strong increase in the scattered intensity with rising temperature can be observed. In addition there is a small increase in the long spacing with increasing temperatures.

The effect of cooling rate after the annealing of drawn fibres on the small-angle scattering is demonstrated in Fig. 14. First, a decrease of about 10 to 15% in the maximum intensity is observed in the case of slowly ($6^{\circ}\,C\,h^{-1}$) cooled samples in comparison with air-quenched fibres. The second

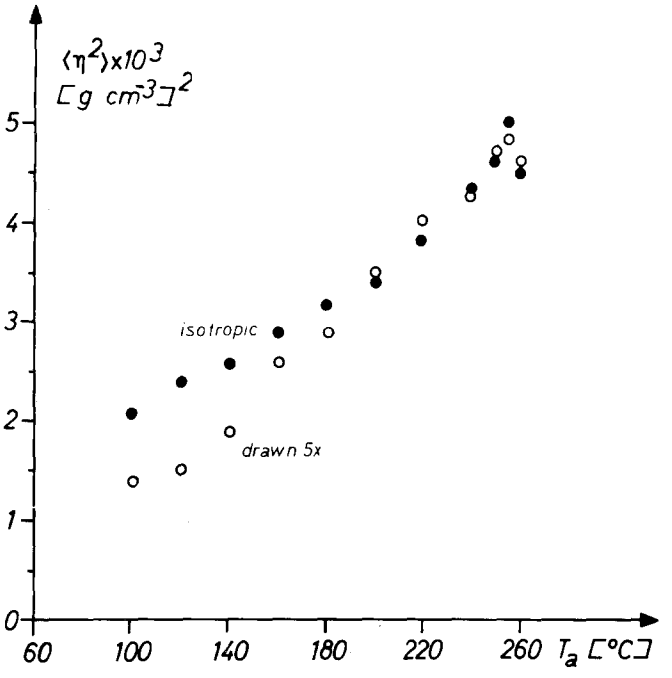

Figure 11 The dependence of the mean square density fluctuation $\langle \eta^2 \rangle$ on the annealing temperature T_a for drawn (○) and undrawn (●) samples.

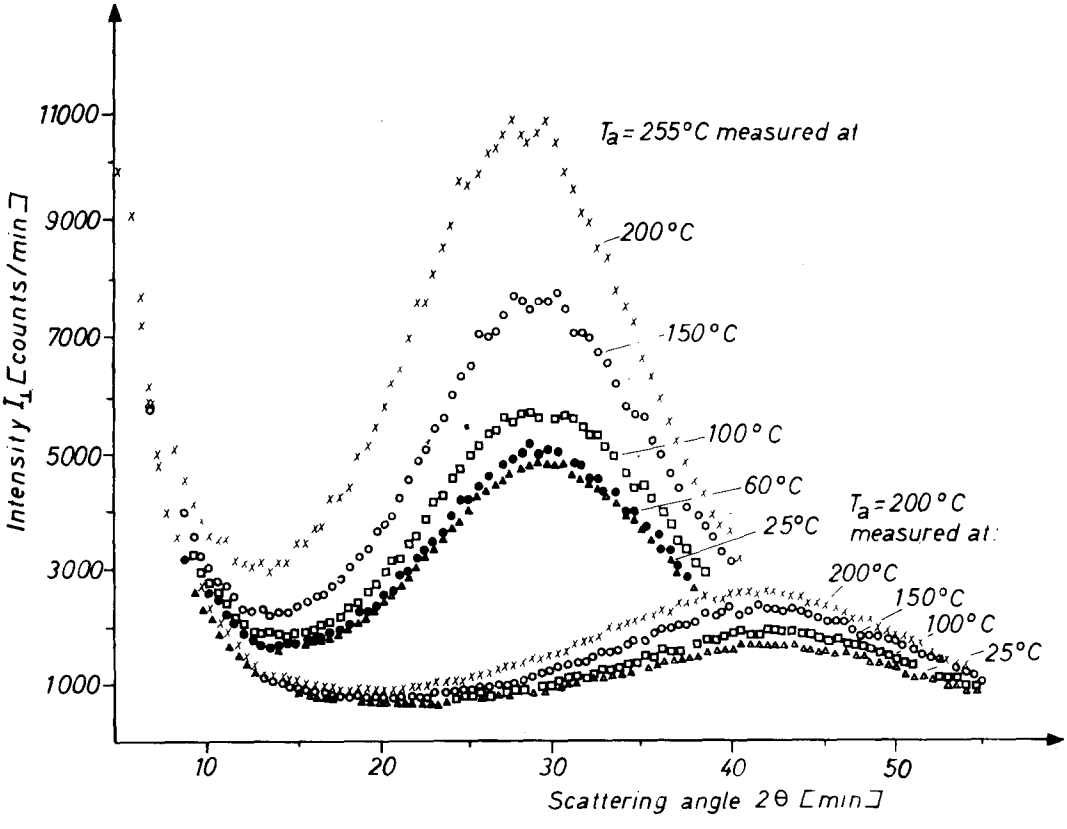

Figure 12 SAXS curves $I_\perp(\theta)$ of drawn PET samples measured at various temperatures. The samples have been annealed for 6 h at $T_a = 200$ or 255° C respectively, before measuring. Fibre axis perpendicular to camera slit.

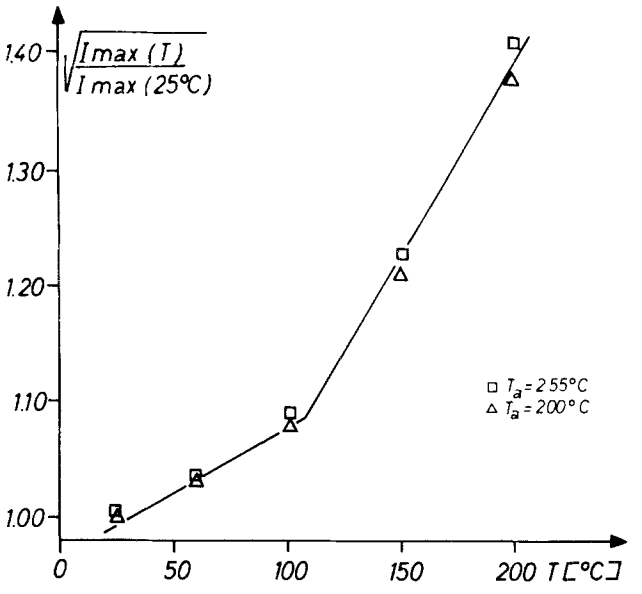

Figure 13 Dependence of peak intensity of the small-angle reflections on measurement temperature.

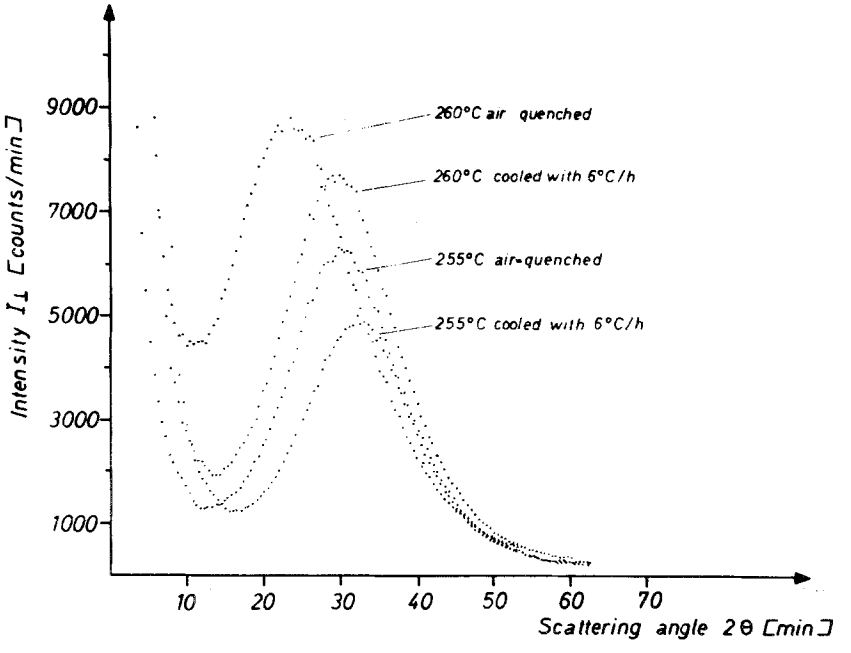

Figure 14 SAXS curves $I_\perp(\theta)$ of drawn PET annealed at 255 and 260° C and cooled at different rates after annealing.

pronounced effect is a shifting of the intensity maximum to higher scattering angles due to slow cooling. This change in the maximum intensity position corresponds to a decrease in the long spacing of about 15% for $T_a = 260°$ C and about 10% for $T_a = 255°$ C.

The scattering intensity is also very sensitive to strain or stress, as can be seen from the scattering curves in Fig. 15. The measurements carried out by Müller [27] on 1 mm thick PET sheets drawn five times and annealed at 260° C for 6 h have shown that the SAXS intensity rises sharply and reversibly when the sample is under strain (5 to 7% deformation) at the time of measurement. If the strain is more than 5 to 7%, the scattering power increases further but is no longer fully reversible.

A similar result has been obtained by Zhurkov

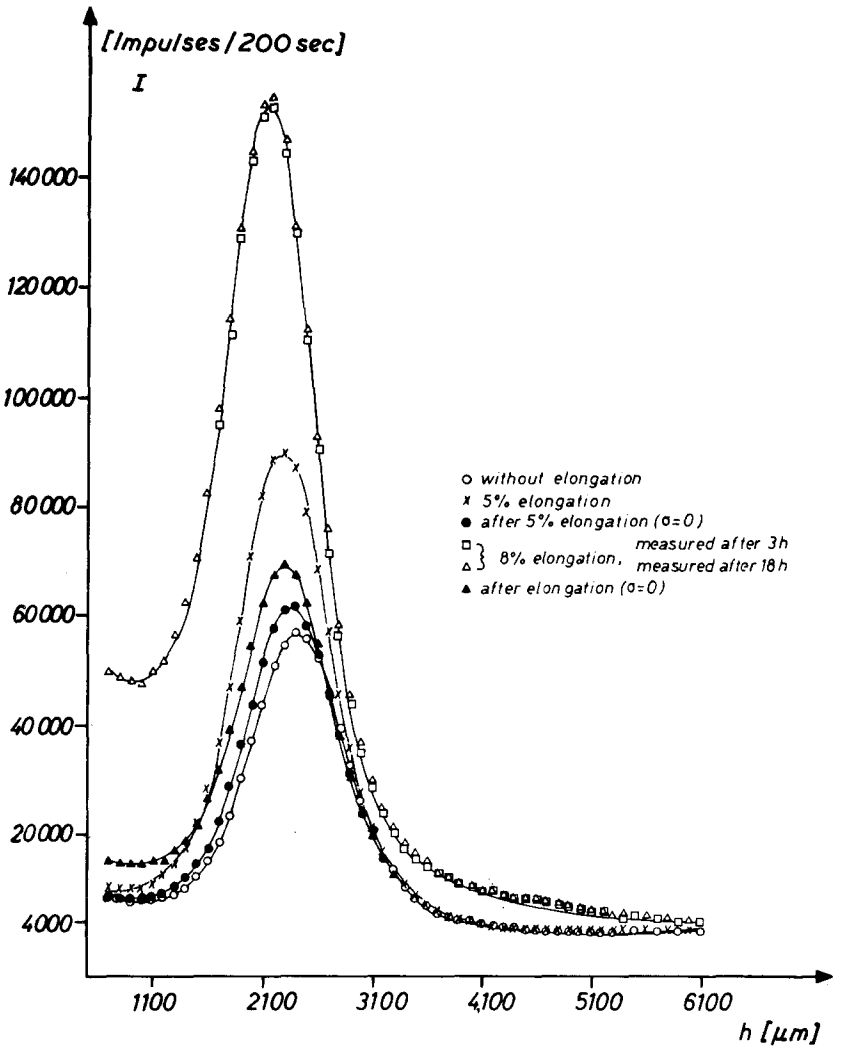

Figure 15 SAXS curves $I_{\perp}(\theta)$ of drawn PET film and PET film annealed at 260° C measured under strain. The parameter of elongation is indicated. (According to measurements of N. Müller.) $h = 2.2 \times 10^5 \tan 2\theta$.

et al. [28] for nylon 6 films. They used a 700% drawn film and measured the SAXS intensity under tension (with 12, 24 and 31% deformation). The scattering power increased continuously and reversibly.

3.2. Wide-angle X-ray scattering and apparent crystallinity

For further characterization of the structure of the studied samples, X-ray wide-angle patterns were taken. Fig. 16a to g show the improvement of order with increasing annealing temperature [9, 29–31]. Some of the relevant features of the X-ray patterns will be discussed later. For the purpose of determining the apparent crystallinities we were primarily interested in the d values of the net planes. From scattering patterns calibrated by SiO_2 powder, the dependence of the net plane distances of the main reflections on annealing temperature was measured. The results are plotted in Fig. 17. No systematic variation in d has been observed for crystallization temperatures above $T_a = 140°$ C. At the lowest annealing temperature (100° C) a small increase in some crystal plane distances was found. Therefore, for samples annealed at 100° C a value of $\rho_c = 1.484\,g\,cm^{-3}$ was used instead of $\rho_c = 1.515\,g\,cm^{-3}$ for the other samples [17].

The apparent volume fraction w_c of crystallinity was calculated from Equation 1 using the measured density values. The results are given in Table I and plotted in Fig. 18. It is quite obvious that the

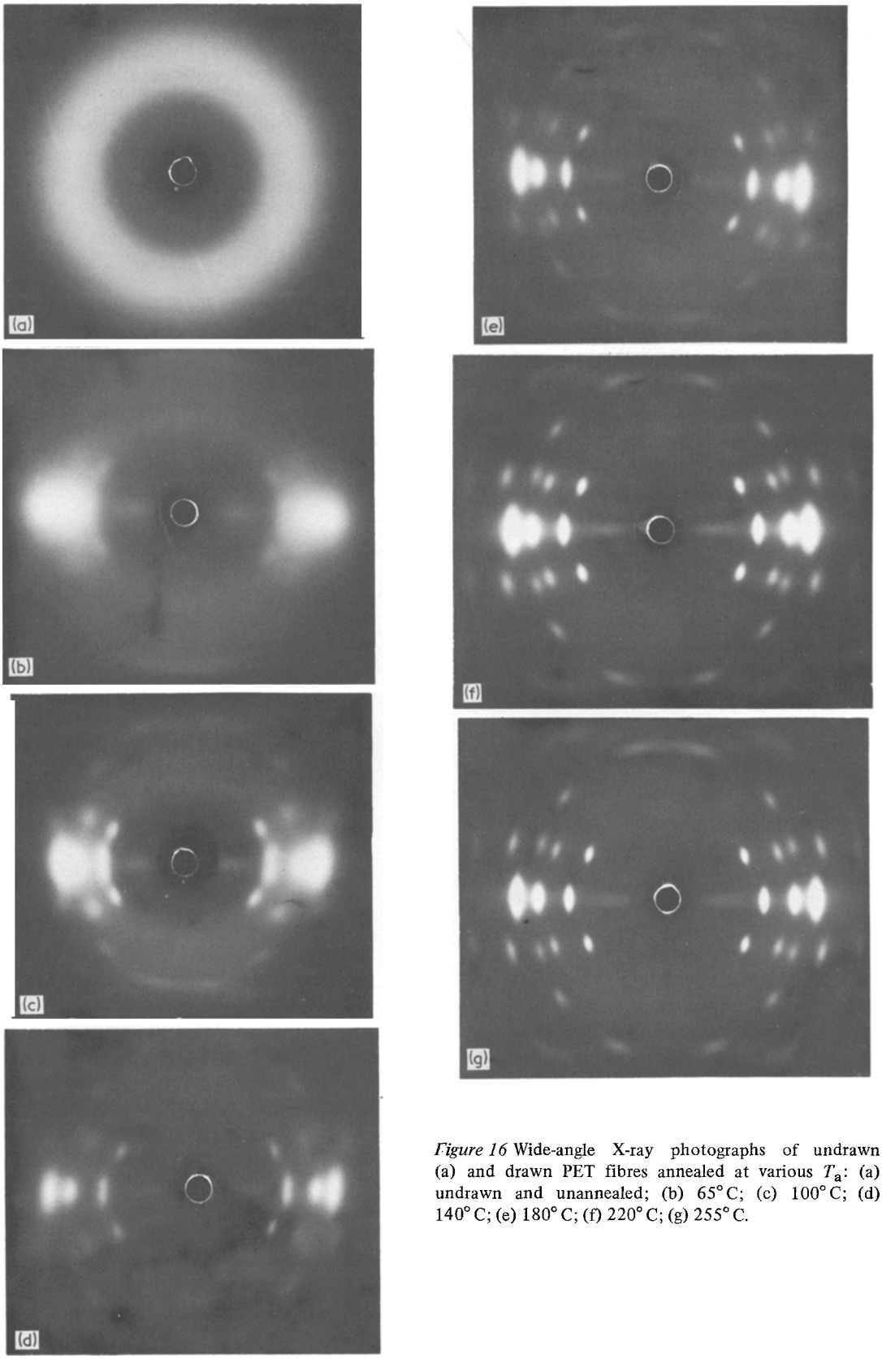

Figure 16 Wide-angle X-ray photographs of undrawn (a) and drawn PET fibres annealed at various T_a: (a) undrawn and unannealed; (b) 65° C; (c) 100° C; (d) 140° C; (e) 180° C; (f) 220° C; (g) 255° C.

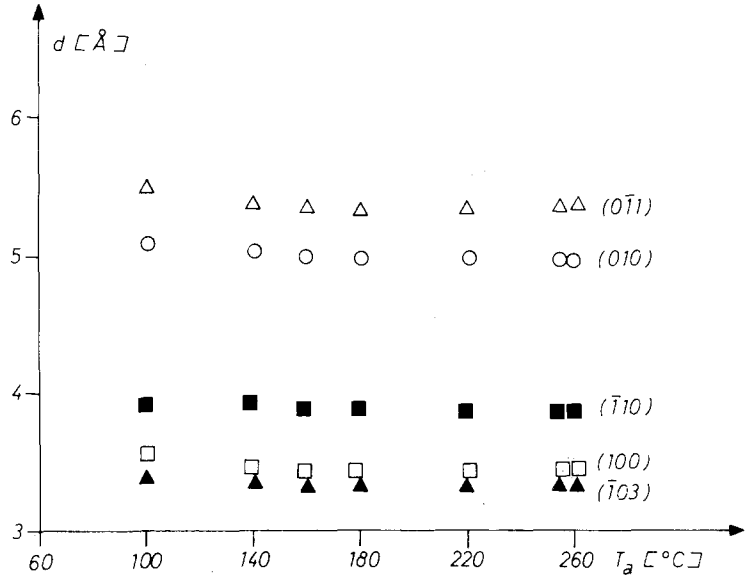

Figure 17 The dependence of distances, d, of various crystal planes (hkl) on annealing temperatures, T_a for drawn PET fibres annealed for 6h in vacuum [17].

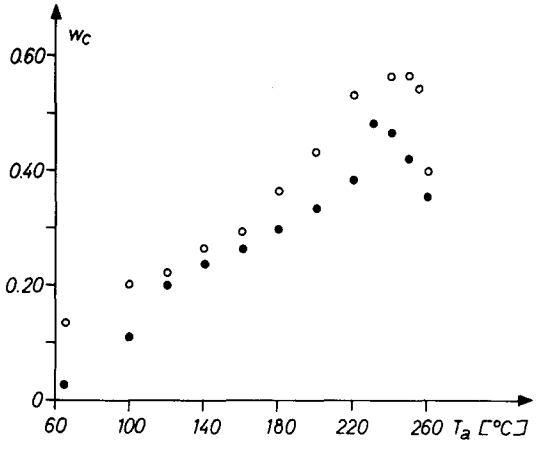

Figure 18 Dependence of apparent crystallinity w_c (from density measurements) on the annealing temperature for undrawn (•) and drawn (○) PET.

TABLE I Structural data for PET bristles

Annealing temperature T_a (°C)	Undrawn					Drawn				
	Density ρ (g cm^{-3})	Cryst. index w_c (from ρ)	Cryst. index w_c (from DSC)	Long period L (Å)	Density fluctuation $\langle\eta^2\rangle \times 10^3$ (g cm^{-3})^2	Density ρ (g cm^{-3})	Cryst. index w_c (from ρ)	Cryst. index w_c (from DSC)	Long period L (Å)	Density fluctuation $\langle\eta^2\rangle \times 10^3$ (g cm^{-3})^2
Unannealed	1.334	0.03	–	–	–	1.356	0.13	–	–	–
100	1.353	0.13	–	132	2.1	1.368	0.23	–	–	1.4
120	1.370	0.20	–	132	2.4	1.372	0.22	–	110	1.5
140	1.375	0.23	0.30	132	2.6	1.380	0.26	0.40	113	1.9
160	1.379	0.25	0.34	135	2.9	1.385	0.30	0.43	115	2.3
180	1.387	0.30	0.35	141	3.2	1.396	0.35	0.44	117	2.9
200	1.393	0.33	0.35	151	3.4	1.411	0.43	0.45	124	3.5
220	1.403	0.39	0.35	156	3.9	1.429	0.53	0.47	131	4.1
240	1.420	0.48	0.42	177	4.4	1.434	0.56	0.51	145	4.3
250	1.417	0.46	0.41	193	4.7	1.435	0.56	0.51	161	4.8
255	1.411	0.43	0.43	264	5.1	1.430	0.54	0.46	176	4.9
260	1.397	0.36	0.33	294	4.6	1.406	0.40	0.38	225	4.7

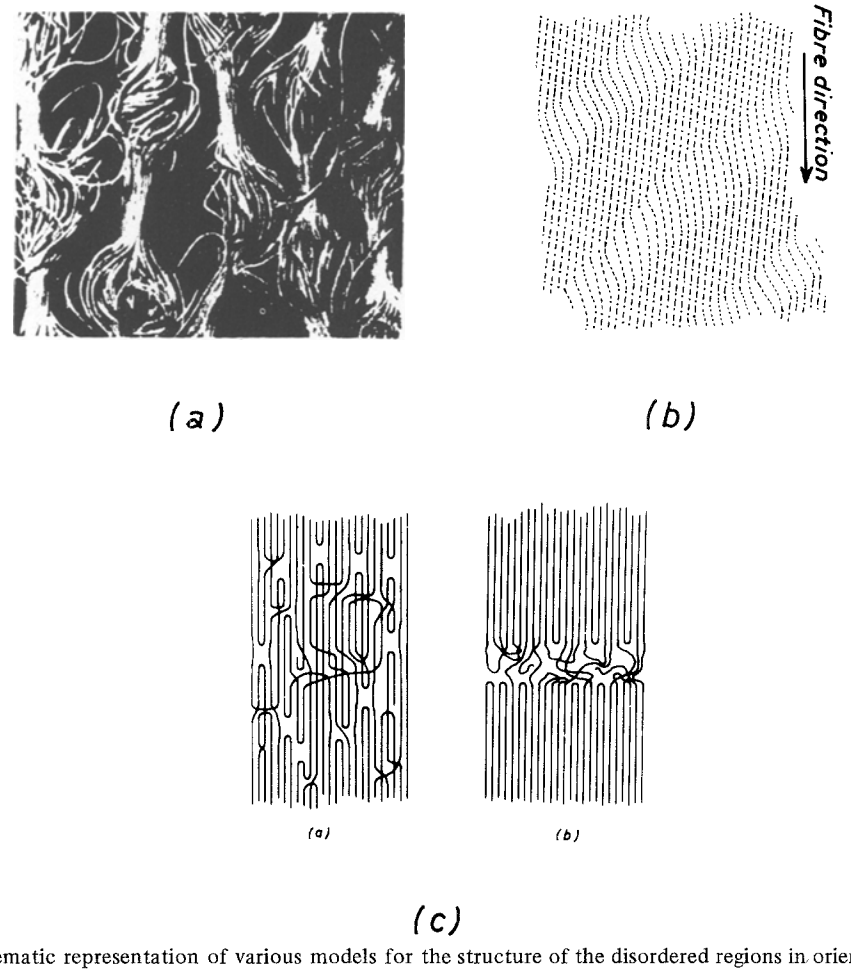

Figure 19 Schematic representation of various models for the structure of the disordered regions in oriented polymers: (a) the fringed micelle model [34]; (b) model of Bonart [35]; (c) model proposed for the effect of annealing on the structure of drawn polymers [21, 38].

crystallinity index is lower for undrawn fibres than for drawn samples. The value of w_c increases continuously with increasing annealing temperature. For comparison, Table I also includes the degree of crystallinity calculated from the DSC data, which will be described in more detail in Part 2. The agreement of w_c values obtained by the two methods is rather poor, especially for the drawn samples annealed at temperatures below 220° C. Such discrepancies due to drawing and orientation are well known for other polymers [32, 33]. It should be noted, however, that the disagreement is much higher, if the conventional value for ρ_c (1.455 g cm^{-3}) is used.

4. Discussion

4.1. The nature of the disordered region in the semicrystalline oriented PET

Various models have been proposed for the morphological structure of PET in the oriented state. Some of them are presented in Fig. 19. The model of Statton [34], shown in Fig. 19a is based on the fringed micelle assumption. Another model explaining the structure of oriented PET is suggested by Bonart [35] (Fig. 19b). In both models a regular alternation of ordered and disordered regions is assumed and the phenomenon of the long-spacing diffraction can be explained satisfactory without taking into account the possibility of chain folding. The meander model of Pechhold [36] belongs to the same group of models.

On the other hand, chain folding can be taken into account as proposed by Bonart and Hosemann [37]. Fig. 19c shows a model, as proposed by Fischer *et al.* [21, 38], for demonstrating the structural changes taking place during annealing of polyethylene. Other models exist [39, 40] which will not be discussed here.

We believe that chain folding does occur to a certain extent during the crystallization in the

oriented state. Apart from other evidence discussed later, the small-angle scattering behaviour under strain seems to indicate folded chains on the surface of the crystallites. As shown in Fig. 15, the scattered intensity increases strongly by extensional deformation and this behaviour can be explained properly by the model proposed by Zhurkov *et al.* [28] assuming a dilution of the noncrystallized regions due to their elongation. In those models which do not include chain folding one would expect to observe a decrease in scattered intensity due to a compression of the amorphous layers followed by a reduction in the density differences between crystalline and amorphous regions. A quantitative analysis of the relationship between SAXS and strain in the case of PET has been carried out and will be published later [27].

Other results indicate the presence of chain folds in oriented crystallized PET. Koenig and Hannon [41] and Prevorsek and Sibilia [42] came to the same conclusion from their infra-red study of drawn annealed PET films. Another possibility of proving this is proposed by Frenkel [6] and is based on the relation between chain folding and thermomechanical properties (force–length–temperature relations). Experimental confirmation of this statement has been found for collagen and poly(vinyl-alcohol) [6, 43]. Similar results were observed for drawn annealed PET fibre [44].

Based on the annealing experiments of drawn PET fibres under relaxed conditions, Dumbleton [45] suggests that chain folding occurs on heating and that the structure of drawn PET resembles that proposed by Dismore and Statton for drawn nylon 66 yarns [46].

On the basis of the indications in the literature and our results from SAXS measurements under strain, the conclusion may be drawn that the crystallization of oriented PET proceeds with folding of macromolecular chains as is typical of the most synthetic polymers.

The SAXS behaviour of the samples studied at different measurement temperatures yields further indications. As already described (Figs. 12 and 13), a strong increase in the scattered intensity with increasing temperature is observed. The dependence of the scattered intensity on measurement temperature can be explained by the difference in the thermal expansion coefficients of crystalline and amorphous regions. From the slope of the $I^{1/2}$–T plot for temperatures above T_g the difference in the thermal expansion coefficients $(\alpha_a - \alpha_c)$ may be estimated [22] according to the equation

$$\sqrt{\frac{I(T)}{I(T_0)}} = 1 + \frac{\alpha_a - \alpha_c}{\Delta\rho(T_0)}(T - T_0). \qquad (6)$$

The value obtained from our results is $(\alpha_a - \alpha_c) \approx 4 \times 10^{-4}\,\mathrm{g\,cm^{-3^o}\,C^{-1}}$ which is in good agreement with results for other polymers. If all the chains ran through the disordered regions it would be difficult to understand how these tie-molecules could show a thermal expansion like an ordinary polymeric liquid. Below 100° C the slope in Fig. 13 is much smaller due to the small difference in thermal expansion coefficients between a glassy polymer and a crystalline polymer. These experiments are of a preliminary character, and more detailed studies must be made in order to prove the effect of partial melting, which has been observed by SAXS intensity measurements in the case of polyethylene and polyoxymethylene [47–49].

4.2. The density of amorphous regions and the dubiousness of the two-phase model

Generally the evaluation of crystallinity from density data according to Equation 1 and the interpretation of physical properties of semicrystalline polymers are based on a two-phase model. In this it is assumed that the polymer consists of an amorphous and a crystalline phase and that the properties of each phase are independent of the presence and amount of the other phase. This assumption also involves a certain conception of the development of the morphological structure. It is believed that the crystals grow with a sharp phase boundary into the amorphous matrix leaving some material untransformed. Because of the importance of the ideas of a two-phase structure it is worth checking their validity. A suitable method for this purpose is the comparison of the mean square density fluctuation $\langle\eta^2\rangle$ measured according Equation 4 with the calculated value. For a two-phase structure consisting of amorphous and crystalline regions with densities ρ_a and ρ_c respectively, the mean square density fluctuation can be calculated from

$$\langle\eta^2\rangle_{cal} = (\rho_c - \rho_a)^2 w_c (1 - w_c), \qquad (7)$$

where w_c is the volume fraction of crystalline material. By means of this method it was proved for polyethylene, both crystallized from solution

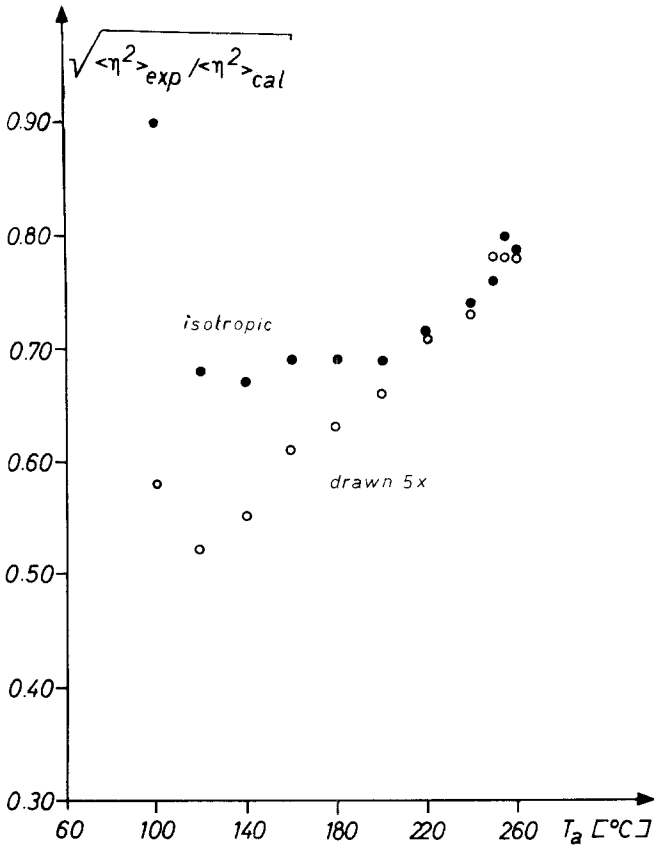

Figure 20 The dependence of the square root of the ratio of experimental and calculated mean square density fluctuations on annealing temperature for undrawn (•) and drawn (○) PET.

[47, 48] or melt [48], and for polyoxymethylene and some co-polymers [49], that the two-phase model is a very good approximation. In the case of drawn polyethylene, however, it failed completely [21, 50].

For drawn and undrawn PET the measured values of the mean square density fluctuation, $\langle\eta^2\rangle_{exp}$, are plotted in Fig. 11. They show a continuous and strong increase with rising temperature. For comparison the square root of the ratio of the measured value of $\langle\eta^2\rangle$ and those calculated according Equation 7 for undrawn and drawn fibres, is plotted in Fig. 20. All values of the ratio are smaller than unity indicating that the conventional two-phase model fails for both the undrawn and drawn PET. For the undrawn bristles the values are signficantly higher up to annealing temperatures of about 220° C. The absolute values of the ratio for undrawn PET differ strongly from those reported by Konrad and Zachmann [25], who found values up to 1.3 at higher annealing temperatures. This disagreement originates mainly from the different values of ρ_c used in both evaluations. For the data plotted in Fig. 20 we used the recently found crystalline density of $\rho_c = 1.515\,g\,cm^{-3}$ [17], whereas the application of Bunn's value $\rho_c = 1.455\,g\,cm^{-2}$ [51] will yield similar data to those published by Konrad *et al.* [25] (for comparison see Fig. 10 of [52]).

The values of the measured mean square density fluctuations $\langle\eta^2\rangle_{exp}$ indicate clearly that the structure of PET both in the drawn and undrawn state cannot be described by a two-phase model with constant values of ρ_c and ρ_a. There are various possibilities for the explanation of these deviations. We will confine ourselves to discussing two effects which seem most likely to occur: (i) there may exist a transition region of finite width between the amorphous and crystalline regions instead of a sharp jump in density, and (ii) either ρ_c or ρ_a or both may depend on the annealing and drawing conditions, thus $\Delta\rho = \rho_c - \rho_a$ is no longer constant.

In conjunction with the first effect, it must be remembered that Equation 7 is based on the assumption of a sharp density transition. If the density changes continuously, as schematically represented in Fig. 21, the application of Equation 7 is not correct. Using the model of Fig. 21 which has been modified by Tsvankin [53] the following

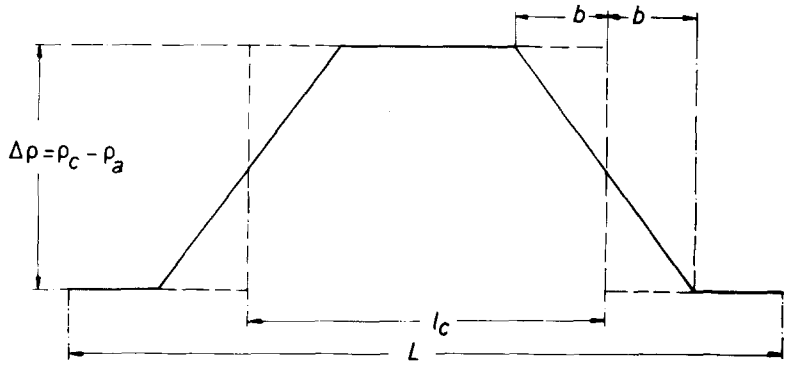

Figure 21 Schematic representation of the electron density distribution along the fibre axis in a semicrystalline oriented polymers.

relation can be derived [54]:

$$\langle \eta^2 \rangle = (\rho_c - \rho_a)^2 \left[w_c(1 - w_c) - \frac{2b}{3L} \right] \quad (8)$$

where $w_c = (l_c/L)$, l_c according to Fig. 21.

From the data of Table I and using Equation 8, we calculated the value b which characterizes the width of the density transition regions. The ratio b/L as a function of the annealing temperature T_a is plotted in Fig. 22. It can be seen that b/L is larger for drawn samples than for undrawn ones and that a maximum is observed for both undrawn and drawn annealed PET. The magnitude of the calculated b values seems to be reasonable. Therefore, the measured density fluctuation may be explained by a finite width of density transition region.

On the other hand, one may also assume that a sharp density transition exists and $\Delta\rho = \rho_c - \rho_a$ is dependent on annealing conditions. At least in principle this question can be decided according to Porod's law [55] by evaluating the outrun of the small-angle intensity curve. Using this method Müller [26] found evidence for the existence of a sharp phase boundary; therefore, the changes of $\Delta\rho$ caused by annealing conditions may be discussed.

The values of $\Delta\rho$ can be calculated from Equation 7 using the measured mean square density fluctuations $\langle \eta^2 \rangle$ if the crystallinity w_c is known. Despite some difficulties which are discussed in more detail in a subsequent paper, the crystallinity index used was derived from DSC measurement. Using these values it is assumed

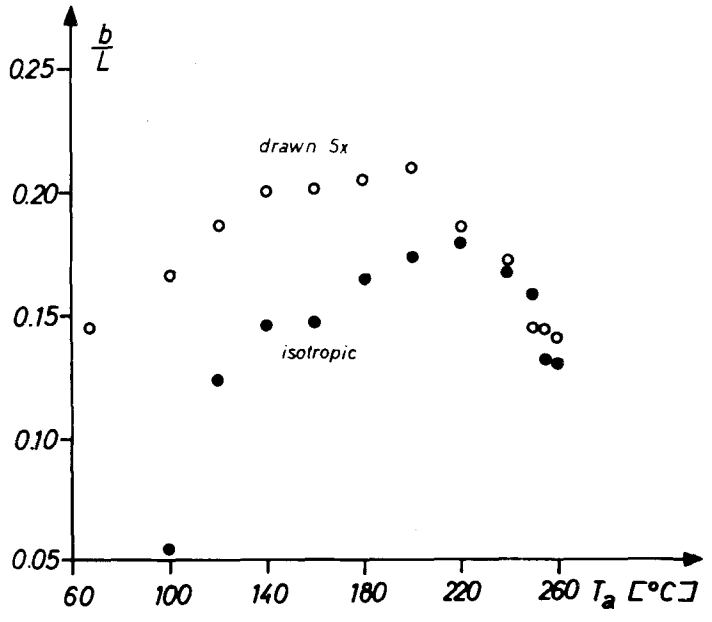

Figure 22 Dependence of the ratio b/L ($2b$ = width of transition region, L = long spacing) on the annealing temperature T_a for undrawn (•) and drawn (○) PET fibres.

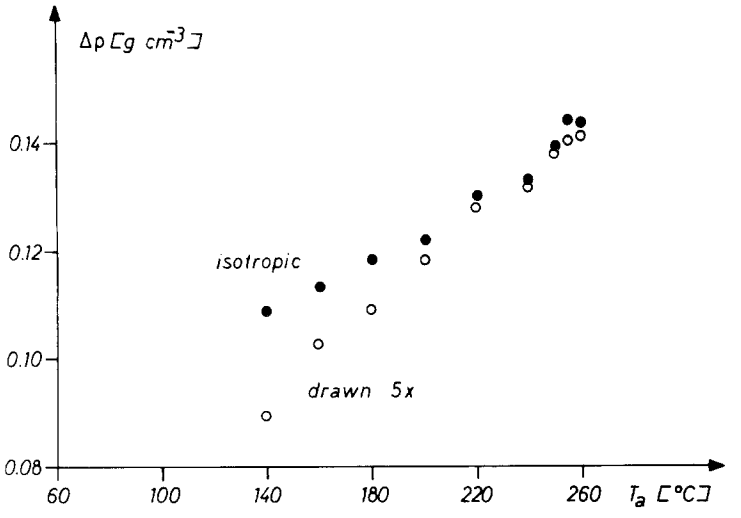

Figure 23 Dependence of the density difference between crystalline and amorphous regions, $\Delta\rho$, on the annealing temperature, T_a, for undrawn (•) and drawn (○) PET fibres.

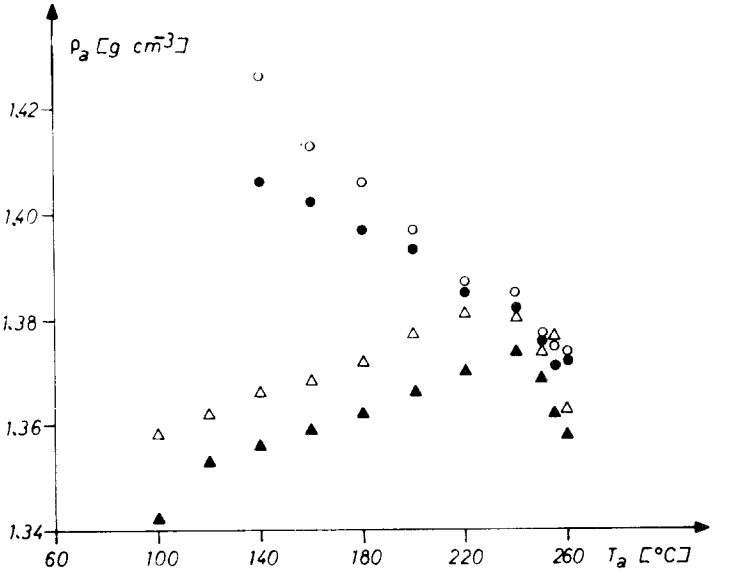

Figure 24 Dependence on annealing temperature of the apparent densities ρ_a of the amorphous regions calculated assuming a constant crystalline density ρ_c. (○ △) Drawn samples, (• △) undrawn samples, (• ○) from DSC data, (▲ △) from density measurements.

that the enthalpy of a semicrystalline sample is the most suitable quantity for characterizing the overall state of order of the polymer. As may be seen from Table I only small changes in w_c (DSC) do occur in contrast to rather large changes in macroscopic density. This observation will be explained on the basis of a model which will be developed later. It is very interesting to note that according to measurements of Konrad and Zachmann [25] the degree of crystallinity evaluated from the correlation function [56] shows almost the same behaviour as w_c (DSC) in Table I, i.e. it depends only slightly on annealing temperature†.

The values of $\Delta\rho$ as calculated from $\langle\eta^2\rangle_{exp}$ and w_c (DSC) are plotted in Fig. 23 as a function of the annealing temperature for drawn and undrawn PET. A continuous increase in $\Delta\rho$ with rising T_a is observed. Such a behaviour has already been found by Fischer *et al.* in the case of drawn polyethylene [21, 50]. The values of $\Delta\rho$ at the highest annealing temperature approach the density difference between ideal crystalline and amorphous phases ($\Delta\rho = 0.182$) without reaching it. At lower annealing temperatures there are very pronounced deviations because either ρ_a or ρ_c or both do not reach their ideal values.

Here the question arises whether the dependence

† In Fig. 9 of [25] the authors did not take into account the fact that the method of Vonk and Kortleve [56] yields the volume fraction of only one phase which may be either the amorphous or the crystalline phase. It is, therefore, likely that the plotted values represent the quantity $(1 - w_c)$.

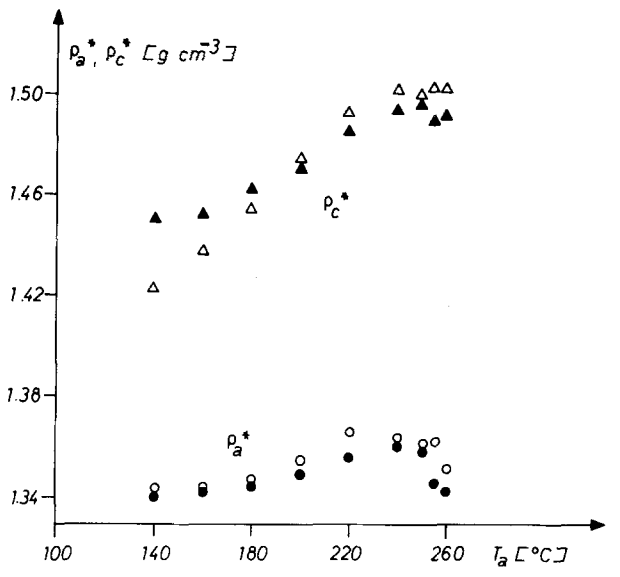

Figure 25 The effective densities ρ_1^* and ρ_c^* of the amorphous and crystalline regions, respectively, in drawn (○ △) and undrawn (● ▲) PET samples.

of $\Delta\rho$ on annealing temperature is completely due to the change of the density ρ_a of the amorphous regions. Assuming ρ_c to be constant and equal to the ideal value $\rho_c = 1.515\,\mathrm{g\,cm^{-3}}$ [17] one can calculate an apparent amorphous density ρ_a^* by two methods. Starting from the values of $\Delta\rho$ evaluated from Equation 7, ρ_a^* is obtained by

$$\rho_{a,1}^* = \rho_c - \Delta\rho. \tag{9}$$

On the other hand ρ_a^* can also be calculated from the measured values of the mean density and of the mean square density fluctuation:

$$\rho_{a,2}^* = \bar{\rho} - \frac{\langle\eta^2\rangle_{exp}}{\rho_c - \bar{\rho}}. \tag{10}$$

The results are plotted in Fig. 24. Obviously there are tremendous discrepancies between the values of ρ_a^* obtained by the two methods, especially for samples annealed at temperatures below 240° C. They are due to the fact that the scattering power of the samples changed dramatically, see Fig. 3, whereas the crystallinity index showed rather small changes.

The results of Fig. 24 indicate that the assumption of a constant ρ_c does not yield a self consistent model. Therefore, we decided to take into account the variability of the apparent crystalline density ρ_c^*.

The values of ρ_a, ρ_c and w_c can be calculated using three independent experimental methods. Applying the data for w_c from DSC measurements and the values of mean square density fluctuation $\langle\eta^2\rangle_{exp}$ as well as the experimentally determined density $\bar{\rho}$ (Table I) the values of ρ_c^* and ρ_a^* as function of annealing temperature were calculated according to the following equations [9] which can be derived by combining Equations 1 and 2:

$$\rho_c^* = \bar{\rho} + \sqrt{\left[\left(\frac{1-w_c}{w_c}\right)\langle\eta^2\rangle_{exp}\right]} \tag{11}$$

$$\rho_a^* = \bar{\rho} - \sqrt{\left[\left(\frac{w_c}{1-w_c}\right)\langle\eta^2\rangle_{exp}\right]}. \tag{12}$$

The data for undrawn and drawn PET are plotted in Fig. 25. The values for ρ_a^* for both undrawn and drawn material vary over a narrow range (1.341 to 1.364) near to the conventionally adopted value of amorphous PET (1.333) showing a small maximum at T_a of about 220 to 240° C. The slight variations of ρ_a may be due to the constraint of the non-crystalline sequences by the crystallites. According to Fig. 25 this densifying effect is slightly larger in drawn material.

In contrast to the behaviour of ρ_a^*, the density of crystalline regions ρ_c^*, changes very strongly – between 1.423 and 1.503 with increasing T_a (Fig. 25). At higher annealing temperatures, the values of ρ_c^* become larger and remain almost constant above 240° C. A similar situation has been already observed by Fischer *et al.* on polyethylene [21, 50] and has already been correlated to the appearance of defects during stretching.

The nature of these defects can be visualized by taking into account four other effects described above: (i) the increase of sharpness of the wide-angle reflections with increasing T_a (see Fig. 16a

to g); (ii) sharpening of the small-angle layer lines (see Fig. 2), (iii) the approximate constancy of the DSC crystallinity index (see Table I); and (iv) the constancy of the net plane spacings above T_a = 140° C (see Fig. 17).

The broadening of the crystal reflections can either be due to lattice distortions or to crystalline size effects. Starting from the close packing principle of Kitaigorodsky [58] one may assume that in the ideal crystal the most dense packing of the PET molecules is realized. There is no space available for introducing paracrystalline distortions without expanding the average crystal unit cell dimensions. Since the net plane spacings are independent of annealing temperature, we conclude that the broadening of the reflections is mainly due to a mosaic block structure of the crystalline layers [59]. Near the grain boundaries, lattice vacancies are introduced which reduce the effective density ρ_c of the crystalline layers (see Fig. 26). This assumption is supported by the results of line width measurements which will be described in Part II of the paper. The size of the mosaic blocks is larger, the higher the annealing temperature. Starting from block dimensions in the region of 50 Å (at $T_a = 180°C$ [60]) a rough estimation shows that the corresponding value of ρ_c^* is obtained by assuming that the fraction of vacancies in the grain boundary is about one tenth of the number of lattice points in the boundary. This seems to be a reasonable number. With increasing annealing temperature not only the lateral size of the mosaic blocks increases, but also their longitudinal order (see Fig. 2 and the discussion below). On the other hand, the contribution of the grain-boundary energy to the overall enthalpy of the sample is small compared with the energy increase due to non-trans conformations of the molecules in the amorphous regions. Therefore, the DSC crystallinity index remains almost constant with change in annealing temperature, whereas the density increases by means of the increasing mosaic block size. The constancy of "crystallinity" is also reflected in other properties, e.g. density correlation function [25] and swelling [57].

4.3. The development of microstructure during annealing

With regard to the dependence of microstructure on annealing conditions two pronounced effects were observed: (i) a tremendous increase in the integrated scattered intensity; and (ii) a change in the shape of the meridional small-angle reflections. The origin of the first effect has been discussed above. From the small-angle patterns of Fig. 1 and the photometer traces of Fig. 2 it can be concluded that the microstructure can be described in terms of a paracrystalline layer lattice, which is characterized by various kinds of longitudinal (along the fibre axis) and lateral arrangements of crystalline blocks. According to the scattering theory developed by Bonart [62] the width of the meridional reflextions in a direction parallel to the equator is correlated to the average longitudinal fluctuation of the positions of the crystallite blocks. Therefore, the results of Fig. 2 indicate that the microstructure approaches a state of plane parallel layers with increasing annealing temperature. This behaviour is generally observed in drawn polymers: in many cases the development of a layer structure perpendicular to the fibre axis is caused by annealing and has also been demonstrated by electron microscopy, e.g. in the case of polyethylene. Thus

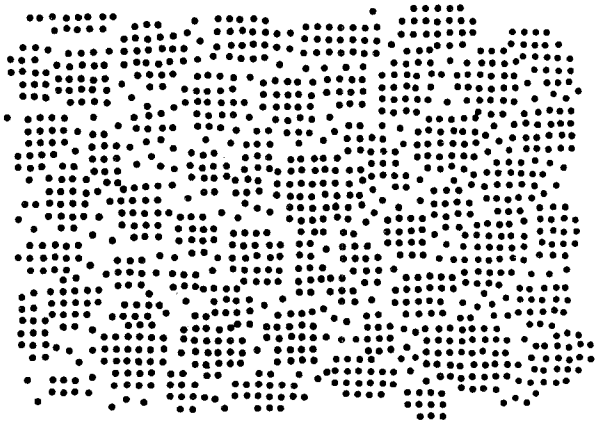

Figure 26 Schematic representation of the cross-section of a crystalline layer with lattice vacancies caused by a mosaic block structure (after R. Hosemann [59]).

changes in shape of the meridional reflections can be interpreted as the improvement of the longidudinal order of neighboured crystallite blocks. There are no distinct structure units such as fibrils in the direction of the fibre axis, however. If this were the case one would expect strong equatorial scattering, which is completely absent. Careful investigations [24] have shown that the continuous scattering around the primary peak is due to foreign heterogeneities of the PET and does not deform if the samples are oriented. From the small-angle studies no evidence of a fibrillar structure can be obtained. Electron microscopic studies do not show any indication of fibrillar structure of the annealed PET samples either [63], although after breaking and dispersion of fragments a fibre morphology is found. If a fibre structure is already present in the unbroken sample, density fluctuation perpendicular to the chain direction must be very small.

Very often the existence of four-point small-angle patterns has ben reported for annealed drawn PET [28, 35, 60]. We observed that only at the highest annealing temperature did first indications of a four-point diagram exist. Some additional experiments were carried out with drawn PET films of 1 mm thickness (in the undrawn state) drawn and annealed in the same way as described above. One example of the results is shown in Fig. 27a to d.

Similar results were described by Statton *et al.* [60] many years ago. Our experiments clearly demonstrate that the appearance of a structure responsible for four-point diagrams is correlated with the macroscopic shape of the sample. Preliminary we may conclude: the four-point diagram structure is caused by a staggering of the molecules along (1 0 0) planes. In a sample with rectangular cross-section, a preferred orientation of these planes parallel to the broader surface takes place during stretching the sample. In the bristles with a circular cross-section, however, a random texture

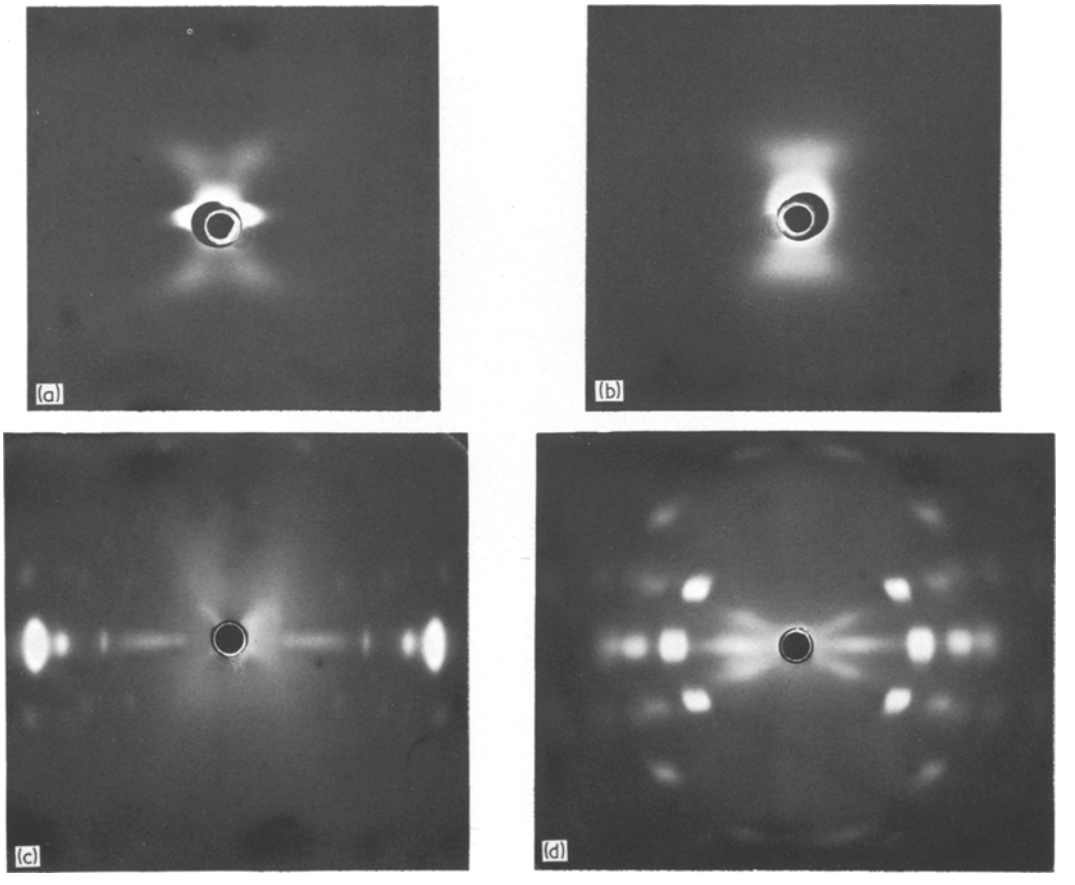

Figure 27 Small-angle (a and b) and wide-angle (c and d) X-ray photographs of drawn and annealed (6 h at 240° C *in vacuo*) PET films. The incident beam is perpendicular to the small or wide side of the film. The drawing direction is vertical.

orientation is observed and, therefore, no largely extended crystalline layer with the staggered conformation can be developed.

It has been found that the chains are tilted 5° with regard to the fibre axis [31, 35, 51]. Since both the tilt and degree of staggering of the molecules depend strongly on annealing temperature it may be assumed that both effects are correlated. A detailed description of staggering and tilting cannot yet be offered, however.

The long spacing L of the drawn and annealed PET shows the generally observed increase with annealing temperature in agreement with other authors [8, 12, 13, 64] but in disagreement with the results of Statton *et al.* [65]. The plot in Fig. 4 shows that the value of L of drawn PET at a given annealing temperature is considerably lower than that of isotropic PET crystallized at the same temperature. In a qualitative manner this effect can be explained on the basis of the influence of strain or stress on the melting point. From Flory's theory [1] it is known that elongation of a polymer in the amorphous state increases its free energy and the melting point of the crystals will accordingly be increased. Since the long spacing depends on supercooling, according to the kinetic theory of crystallization, a decrease in L at constant crystallization temperature may be expected. Theoretical considerations along these lines have been developed by Kobayashi *et al.* [4] and by Krigbaum *et al.* [2].

The independence of the long spacing L on time, see Fig. 5, is in contrast to the behaviour of other polymers, where in many cases a long term increase in L is observed to be characterized by isothermal thickening. Our observations agree, however, with the results of investigations concerned with the crystallization kinetics of drawn PET [67–69]. It was shown there that the main changes in crystallinity, either measured by X-ray, density [68] or shrinkage behaviour [69], took place in small fractions of a minute or even in some hundred milliseconds. Evidently during this crystallization a certain long spacing is developed depending on crystallization temperature and no further changes occur.

In the case of undrawn PET a decrease in L during the secondary crystallization has been observed [19]. As a comparison of the scattering curves in Figs. 3 and 10 shows, the long spacing reflection in the case of drawn material is much better defined. Therefore, changes of the particle factor $(B(s))^2$ which may change during the secondary crystallization will not effect the angle position of the maximum of the scattering curve but only its intensity, as was observed.

Summarizing the results of our structure studies, we may develop the following conception about the effect of annealing temperature on the structure of drawn PET: the main effect is the increase in order within the crystalline layers arranged perpendicular to the fibre direction. The higher the annealing temperature the larger are the dimensions of the mosaic blocks both parallel and perpendicular to the chain axes. In addition, the longitudinal mutual order of the mosaic blocks is improved. Consequently, the effective density ρ_c^* of the crystalline regions increases. We believe that the lateral growth of the mosaic blocks is only possible by additional chain folding and staggering, since growth is hindered by chains which are already incorporated in other mosaic blocks. The staggering causes an increase in available space in the amorphous regions. The chain sequences in the noncrystallized regions are rather constrained and, therefore, the effective density ρ_a^* of the amorphous regions approaches the value of the ideal state only at rather high annealing temperatures. A rough schematic drawing of the structure at low and high annealing temperatures is given in Fig. 28.

We do not believe that the results of the mechanism of crystallization of PET in the oriented state can be explained on the basis of Keller's model [7]. It seems that there exist a very large

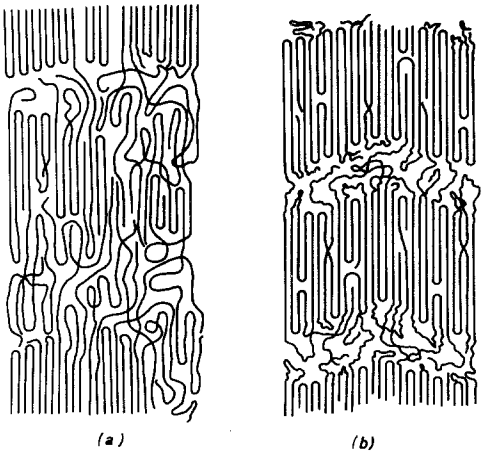

Figure 28 Schematic representation of changes of the structure of oriented PET during crystallization at different temperatures: (a) after annealing at lower T_a; (b) after annealing at higher T_a.

number of nuclei and during crystallization an improvement in order around the nuclei occurs. Our conclusions show some similarities to the model proposed by Yeh and Geil [8]; we believe, however, that the important question of the structure in the amorphous state is still unsolved in the case of PET. In order to develop an acceptable model for the crystallization behaviour of PET this problem must be studied in more detail. At present the overwhelming majority of experimental results do not indicate the presence of bundle-like, ball-like, or meander structures in a truly amorphous polymer [69, 70] or in a polymer melt [71]. This statement does not exclude the possibility of the formation of highly distorted paracrystalline nuclei at the beginning of crystallization or even during stretching (see Fig. 16b).

5. Conclusions

(1) The density difference between crystalline and amorphous layers is caused by chain folding of some of the chains at the boundary of the crystallites and not by different inclination of the chain axes.

(2) The "degree of crystallinity" of PET cannot be calculated from density measurements using the conventional values of ρ_c and ρ_a.

(3) The effective densities ρ_c^* and ρ_a^* of the crystalline and amorphous regions depend strongly on crystallization temperature. The effect is more pronounced in drawn material. Alternatively it may be assumed that there are no sharp transition regions between the ordered and disordered regions.

(4) The sharpening of the wide-angle reflections with increasing crystallization temperature is mainly due to an increase in the size of the mosaic blocks which build up the crystalline layers. The longitudinal mutual order of the mosaic blocks also increases. The low effective density ρ_c^* of the crystalline layers is due to lattice vacancies caused by the grain boundaries of the mosaic blocks.

(5) During crystallization, staggering of the crystallized stems of chains occurs leading to four-point small-angle diagrams if the sample has a suitable macroscopic shape.

(6) The crystallization mechanism is supposed to be similar to that proposed by Yeh and Geil [8], although it is believed that from these results no conclusions can be drawn with regard to the structure and chain conformation in truly amorphous PET.

Acknowledgement

This work was supported in part by the "Sonderforschungsbereich 41 der Deutschen Forschungsgemeinschaft" and in part by the "Alexander von Humboldt-Stiftung". The authors gratefully acknowledge this support. One of us (S.F.) is indebted to Alexander von Humboldt-Stiftung for the Fellowship. We also wish to thank Dr J. H. Wendorff and Dr G. F. Schmidt for helpful advice on and kind interest in this work.

References

1. P. J. FLORY, *J. Amer. Chem. Soc.* 78 (1956) 5222; see also L. MANDELKERN, "Crystallization of Polymers" (McGraw-Hill, New York, 1964) p. 166 f.
2. W. R. KRIGBAUM and R. J. ROE, *J. Polymer Sci.* **A-2** (1964) 4391.
3. R. J. ROE and W. R. KRIGBAUM, *J. Appl. Phys.* **35** (1964) 2215.
4. K. KOBAYASHI and T. NAGASAWA, *J. Macromol. Sci.-Phys.* **B4** (1970) 331.
5. A. ZIABICKI, *Kolloid-Z.u.Z. Polymere* **252** (1974) 207; 252 (1974) 433.
6. S. YA. FRENKEL, Supplement III in the Russian translation of P. H. Geil "Polymer Single Crystals" (Moscow, 1968).
7. A. KELLER and M. J. MACHIN, *J. Macromol. Sci. -Phys.* **B1** (1967) 41.
8. G. S. Y. YEH and P. H. GEIL, *J. Macromol. Sci. -Phys.* **B1** (1967) 251.
9. R. BONART and F. SCHULTZE-GEBHARDT, *Angew. Makromol. Chem.* **22** (1972) 41.
10. A. PETERLIN, in "Man Made Fibers", edited by H. F. Mark, S. M. Atlas and E. Cernia (Interscience, New York, 1967); *J. Polymer Sci.* **A-2** 7 (1969) 1151.
11. I. M. WARD, "Mechanical Properties of Solid Polymers" (Interscience, New York, 1971).
12. R. J. SAMUELS, "Structured Polymer Properties" (John Wiley, New York, 1974).
13. C. D. ARMEDIADES, I. KURIYMA, J. M. ROE and E. BAER, *J. Macromol. Sci. -Phys.* **B1** (1967) 777; J. H. DUMBLETON and T. MURAYAMA, *Kolloid Z.u.Z. Polymere* **220** (1967) 41; *ibid* **228** (1969) 54; J. P. BELL and T. MURAYAMA, *J. Polymer Sci.* **A-2** 7 (1969) 1059; R. A. DUCKETT, S. RABINOWITZ and I. M. WARD, *J. Mater. Sci.* **5** (1970) 909; D. SIMOV, S. FAKIROV, M. MICHAILOV and P. PETRENKO, *Vysokomolek. Soedin* **A15** (1973) 1775 (translated in *Polymer Sci. USSR* **15** (1973) 1998).
14. J. BRANDRUP and E. H. IMMERGUT, "Polymer Handbook" (Interscience, New York, 1966).
15. O. KRATKY, J. PILZ and P. J. SCHMITZ, *J. Colloid Interface Sci.* **21** (1966) 24.

16. E. W. FISCHER and G. F. SCHMIDT, *Angew. Chem.* **74** (1962) 551.
17. S. FAKIROV, E. W. FSICHER and G. F. SCHMIDT, *Makromol. Chem.* **176** (1975) 2459.
18. C. W. SMITH and M. DOLE, *J. Polymer Sci.* **20** (1956) 37.
19. H. G. ZACHMANN and G. F. SCHMIDT, *Makromol. Chem.* **52** (1962) 23.
20. O. POROD, *Fortschr. Hochpolym. Forschung* **2** (1961) 363; R. BONART, *Kolloid Z.u.Z. Polymere* **211(1966)** 14.
21. E. W. FISCHER, H. GODDAR and G. F. SCHMIDT, *Makromol. Chem.* **118** (1968) 144.
22. E. W. FISCHER and F. KLOOS, *J. Polymer Sci.* **B8** (1970) 685.
23. D. HEIKINS, P. H. HERMANS, P. F. VAN VELDEN and A. WEIDINGER, *ibid* **11** (1953) 433.
24. J. H. WENDORFF and E. W. FISCHER, *Kolloid Z.u.Z. Polymere* **251** (1973) 884.
25. G. KONRAD and H. G. ZACHMANN, *ibid* **247** (1971) 851.
26. E. H. MULLER, *Colloid Polymer Sci.* **252** (1974) 696.
27. E. W. FSICHER and N. MULLER, unpublished data.
28. S. N. ZHURKOV, A. I. SLUTSKER and A. A. YASTREBINSKY, *Doklady Acad. Nauk SSSR* **153** (1963) 303.
29. H. G. KILIAN, H. HALBOTH and E. JENCKEL, *Kolloid Z.* **172** (1960) 166.
30. R. BONART, *ibid* **213** (1966) 1.
31. T. ASANO and T. SETO, *Polymer J.* **5** (1973) 72.
32. A. PETERLIN and G. MEINEL, *J. Appl. Phys.* **36** (1965) 3028.
33. E. W. FISCHER and G. HINRICHSEN, *Kolloid Z.u.Z. Polymere* **213** (1966) 28.
34. W. O. STATTON, *J. Polymer Sci.* **41** (1959) 143.
35. R. BONART, *Kolloid Z.u.Z. Polymere* **199** (1964) 136.
36. W. PECHHOLD, *ibid* **228** (1968) 1; **231** (1969) 418; W. PECHHOLD and S. BLASENBREY, *ibid* **241** (1970) 955.
37. R. BONART and R. HOSEMANN, *Makromol. Chem.* **39** (1960) 105.
38. E. W. FISCHER and H. GODDAR, IUPAC-Symposium Macromol. (Prague 1965) p. 7; *J. Polymer Sci.* **C 16** (1969) 4405.
39. K. HESS and H. KIESSIG, *Z. Phys. Chem.* **193** (1944) 196.
40. J. W. C. HEARLE, *J. Appl. Polymer Sci.* **7** (1963) 1175.
41. J. L. KOENIG and M. J. HANNON, *J. Macromol. Sci.* **B1** (1967) 119.
42. D. C. PREVORSEK and J. P. SIBILIA, *ibid* **B5** (1971) 617.
43. S. YA. FRENKEL and B. M. GINSBURG, International Symposium on Macromolecular Chemistry Bruxelles 1967, preprint 4193.
44. D. SIMOV, S. FAKIROV and M. MIKHAILOV, *Kolloid Z.u.Z. Polymere* **238** (1970) 521; International Symposium on Macromolecules, Leiden 1970, preprint, Vol II p. 681; S. FAKIROV and M. MICHAILOV, *Kolloid Z.u.Z. Polymere* in press.
45. J. H. DUMBLETON, *J. Polymer Sci.* **A2** 7 (1969) 667; *Polymere* **10** (1969) 539.
46. P. F. DISMORE and W. O. STATTON, *J. Polymer Sci. C* **13** (1966) 133.
47. E. W. FISCHER, H. GODDAR and G. F. SCHMIDT, *ibid* **B5** (1967) 619.
48. G. R. STROBL and N. MULLER, *J. Polymer Sci.* **11** (1973) 1219.
49. P. J. HOLDSWORTH and E. W. FISCHER, *Makromol. Chem.* **175** (1974) 2635.
50. E. W. FISCHER, H. GODDAR and G. F. SCHMIDT, *J. Polymer Sci.* **A2** (1969) 37.
51. R. DE DAUBENY, C. W. BUNN and C. J. BROWN, *Proc. Roy. Soc. Lond. A* **226** (1954) 531.
52. E. W. FISCHER, *Progr. Colloid Polymer Sci.* **57** (9175) 149.
53. D. YA. TSVANKIN, *Vsyokomol. Soedin* **6** (1964) 2078, 2038, 2131.
54. H. HESPE, Ph. D. Thesis, Mainz (1968).
55. G. POROD, *Kolloid -Z.* **124** (1951) 83.
56. C. G. VONK and G. KORTLEVE, *Kolloid Z.u.Z. Polymere* **220** (1967) 19; ibid 225 (1968) 124.
57. H. G. ZACHMANN, *Makromol. Chem.* **74** (1964) 29.
58. A. I. KITAIGORODSKY, "Molecular Crystals and Molecules" (Academic Press, New York and London, 1973).
59. R. HOSEMANN, *Polymer 3* (1962) 349.
60. W. O. STATTON and G. M. GODARD, *J. Appl. Phys.* **28** (1957) 1111.
61. L. I. BEZRUK, T. KAWAI and YU. S. LIPATOV, *Polymer J.* **6** (1974) 376.
62. R. BONART, *Kolloid Z.u.Z. Polymere* **194** (1964) 97.
63. S. FAKIROV, D. SIMOV and M. MICHAILOV, *Faserforsch. und Textiltechn.* **22** (1971) 554; I. VOIGT-MARTIN, unpublished data; G. KANIG, *Kunststoffe* **164** (1974) 470.
64. W. O. STATTON, *J. Polymer Sci.* **A2 10** (1972) 1587.
65. W. O. STATTON, J. L. KOENIG and M. HANNON, *J. Appl. Phys.* **41** (1970) 4290.
66. J. E. SPRUIELL, D. E. McCORD and R. A. BEUERLEIN, *Trans. Soc. Reol.* **16** (1972) 535.
67. H. -J. BIANGARDI and H. G. ZACHMANN, unpublished data.
68. F. S. SMITH and R. D. STEWARD, *Polymer* **15** (1974) 238.
69. Symposium on Physical Structure of the Amorphous State ACS-Polymer Meeting, Atlantic City, September 1974.
70. E. W. FISCHER, J. H. WENDORFF, M. DETTENMAIER, G. LIESER and I. VOIGT-MARTIN, *J. Macromol. Sci.- Phys.*, in press.
71. G. LIESER, E. W. FISCHER and K. IBEL, *J. Polymer Sci.* **B13** (1975) 39.

Received 31 October and accepted 17 November 1975.